Research Article Vol. 30, No. 5 / 28 Feb 2022 / Optics Express 6768
Optics EXPRESS

Distributed temperature sensor combining centimeter resolution with hundreds of meters sensing range

JULIEN GASSER,[1] DARYL WARPELIN,[1] FÉLIX BUSSIÈRES,[2] JÉRÔME EXTERMANN,[1] AND ENRICO POMARICO[1,*]

[1]HEPIA, HES-SO, University of Applied Sciences and Arts Western Switzerland, Rue de la Prairie 4, 1202 Geneva, Switzerland
[2]ID Quantique SA, CH-1227 Carouge, Switzerland
*enrico.pomarico@hesge.ch

Abstract: We present a Raman distributed temperature sensor based on standard telecom single mode fibers and efficient polarization-independent superconducting nanowire single photon detectors. Our device shows 3 cm and 1.5 °C resolution on a 5 m fiber upon one minute integration. We show that spatial resolution is limited by the laser pulse width and not by the detection system. Moreover, for long fibers the minimum distance for a measurable temperature step change increases of around 4 cm per km length, because of chromatic dispersion at the Stokes and Anti-Stokes wavelengths. Temperature resolution is mainly affected by the drop in the laser repetition rate when long fibers are tested. On a 500 m fiber, a trade-off of 10 cm and 8 °C resolution is achieved with 3 minutes integration. Fiber-based distributed temperature sensing, combining centimetric spatial resolution with hundreds of meters sensing range, could pave the way for a new kind of applications, such as 2D and 3D temperature mapping of complex electronic devices, particles detectors, cryogenic and aerospace instrumentation.

1. Introduction

Distributed temperature sensing is a technology enabling the real-time measurement of the continuous profile of the temperature along an optical fiber. Nowadays, this technology represents a valid alternative to the installation of localized point sensors and is successfully deployed for many industrial applications, such as oil and gas production, power cable and transmission line monitoring, fire detection in tunnels, as well as for ecological monitoring, such as groundwater source detection, temperature profiling in mine shafts and over water basins.

To achieve temperature sensing over long distances, most distributed temperature sensors (DTSs) use Optical Time-Domain Reflectometry (OTDR), which consists in sending optical pulses into a fiber and analyzing the backscattered light [1]. With respect to the standard OTDR technique, distributed temperature sensing exploits the spectral components of the back-scattered light that are sensitive to temperature. Indeed, the spectrum of the back-scattered light mainly consists in the Rayleigh band, based on photons with the same energy of the input light, in sidebands originated by Brillouin scattering, and in large bands corresponding to Stokes (S) and Anti-Stokes (AS) Raman scattering, showing an energy shift with respect to the input energy. This shift is related to the energy associated to the optical phonon which photons interact with in the fiber cable. The intensity of Raman bands, particularly the AS one, depends on temperature. In a Raman DTS (RDTS) these signals are combined to obtain the profile of the temperature all along a fiber under test (FUT) [2].

RDTSs based on OTDR can easily operate over km sensing distances. Most of the devices reported in literature use multimode fibers to compensate the weak Raman backscattered signal and increase the collection of backscattered photons. However, because of modal dispersion, the

#451699 https://doi.org/10.1364/OE.451699
Journal © 2022 Received 19 Dec 2021; revised 28 Jan 2022; accepted 30 Jan 2022; published 15 Feb 2022

Optics EXPRESS

sensing range of this kind of RDTS is limited to 10-20 km for a spatial resolution of around 1 m and a temperature resolution between 1 and 5 °C [3,4,5,6]. Longer distances have been achieved by using low-losses single mode (SM) telecom fibers [7]. However, most existing OTDR-based DTSs do not achieve spatial resolution better than 1 meter. In fact, even when SM fibers are used, the spatial resolution of a DTS is limited by the response function of the detection system: most DTSs that are commercially available or reported in literature use avalanche photodiode detectors (APDs) in a linear amplification regime with limited timing resolution.

This limitation can be overcome by using superconducting single photon nanowire detectors (SNSPDs) [8,9]. These detectors provide several advantages for a DTS: they typically have low timing jitter (few tens of ps), high broadband efficiency, low dark count rate, and free running operation, providing high spatial resolution, high sensitivity with reduction of measurement times, similar efficiency for S and AS signals, as well as no segmentation of OTDR measurements. SNSPDs can be used for temperature sensing via the use of the photon counting OTDR technique [10], where time-correlations between the launch of a laser pulse and the detection of backscattered photons at the SNSPDs are measured. By using SNSPDs with around 65 ps jitter, Dyer *et al* have shown for the first time a spatial resolution at the cm scale for temperature sensing in standard SM telecom fibers [11]. This result was obtained on a 2.8 m fiber via a setup based on erbium doped amplifiers (EDFAs) to compensate the low efficiency of the adopted SNSPSDs. Polarization diversity receivers were needed to compensate the polarization sensitivity of the detectors. A temperature accuracy of less than 1 °C with an integration time of some seconds has been obtained by Vo *et al* via SNSPD detectors [12]. These results have been obtained with a 2.7 m multimode chalcogenide fiber with a Raman gain coefficient two orders of magnitude larger than that of a silica fiber. In the two afore-mentioned cases, extending the short sensing range to km distances would not be obvious, because of detection inefficiency in [11] and unfeasible hundreds of meters long chalcogenide fibers in [12]. These constraints strongly limit the variety of applications that could take advantage from a DTS with centimetric spatial resolution.

In this work, we expand the potential of high spatial resolution Raman distributed temperature sensing technology by using efficient polarization insensitive SNSPDs: these detectors allow to make a RDTS with a simple optical configuration and achieve a centimetric spatial resolution on hundreds of meters sensing range with short integration times. This could open the way for a new kind of applications, such as 2D and 3D mapping of temperature at centimetric scale of complex electronic, mechanic, cryogenic, and aerospace devices.

2. Methods

As shown in Fig. 1(a), a time to digital controller (TDC) (IdQuantique, ID900 Time Controller) is used to trigger a diode laser (PicoQuant, LDH-P-C-N-1550) to emit pulses at 1548 nm, with 1.5 nm bandwidth full width at half maximum (FWHM), between 50 to 250 ps duration, and around 100 mW peak power. After passing through a 13 nm band-pass filter to reduce Rayleigh noise originated by tails in the laser spectrum, optical pulses are sent into a SM telecom FUT. A standard calorimeter is used to warm up portions of the FUT of the order of 1 m, whereas a custom-made electronic heating system has been developed to warm up localized zones in the FUT of 1 cm length. A circulator deviates the back-scattered light to a Raman WDM-based module (OfLink, RWDMM-456-SM-L-10-FA), separating with a 20 nm spectral window the light at 1450 nm (AS signal, 0.48 insertion loss, 62 dB isolation) from that at 1660 nm (S signal, 0.73 insertion loss, 62 dB isolation). The AS and the S signals are detected by two SNSPDs (ID Quantique, ID281), based on a thin film of amorphous MoSi and mounted in a sorption cryostat working at 0.8 K [13]. The SNSPDs have a detection efficiency in the range of 60 to 70%, a jitter of ~30 to 50 ps and a dark count rate of less than 100 counts per second. Single photon response voltages from SNSPDs are amplified and used as STOP signals for the TDC

Optics EXPRESS

[13]. Importantly, the detectors operate in a latch-free manner and are therefore insensitive to strong back reflections that could disable them or disrupt their free-running operation.

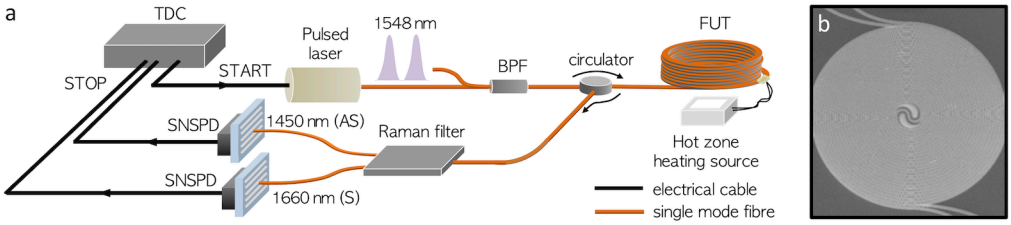

Fig. 1. a) Sketch of the RDTS with centimetric spatial resolution. A Time-to-Digital Controller (TDC), equipped with timed-output signals, triggers a laser, emitting pulses at 1548 nm, which are filtered by a band-pass filter (BPF) and injected via a circulator into a fiber under test (FUT). A 1 cm hot zone on the FUT is produced by an electronic heating source. Back-scattered light is sent to a Raman filter separating the Anti-Stokes signal (1450 nm, AS) from the Stokes one (1660 nm, S). Each Raman signal is then detected by a superconducting nanowire single photon detector (SNSPD). b) A scanning electron microscope (SEM) image showing the spiral geometry of the superconducting nanowire of the polarization independent SNSPDs.

The Raman backscattered light does not have in general a defined polarization. Indeed, the polarization of the pump laser changes with position in the sensing fiber because of the varying birefringence and the polarization-dependent Raman gain [14]. In our case, the adopted SNSPDs are polarization insensitive, as the superconducting nanowire has a spiral geometry (Fig. 1(b)). In addition, all other optical components of the RDTS are polarization independent. We have measured a 2% variation of the detected signal by varying the polarization of the pulses at the input of the FUT. These properties make our RDTS rather insensitive to polarization.

3. Working principle of the RDTS

The number of S and AS photons I_i (with $i = S, AS$) detected per second at a position x in the FUT is given by

$$I_i(x) = \eta_i \Delta f_i P_o D L g_R N_i(T) e^{-\alpha_P x} e^{-\alpha_i x} + DC_i, \tag{1}$$

where η_i is a coefficient including the transmission through the optical components (circulator and Raman module) as well as the SNSPD detection efficiency, Δf_i the bandwidth of the S and AS filters, P_o the peak pump power, D the duty cycle of the pump beam, L the length of the FUT, g_R the Raman gain coefficient (of the order of 1 W^{-1} km^{-1} [15]), α_P and α_i the fiber attenuations per unit length at the pump and Raman wavelengths respectively, and DC_i the dark count rate of the two detectors. $N_i(T)$ is the phonon population at temperature T, which can be described by the Bose-Einstein distribution via the equations

$$N_{AS}(T) = \frac{1}{e^{\frac{\hbar \Omega_{AS,p}}{k_B T}} - 1}, \tag{2}$$

$$N_S(T) = \frac{1}{e^{\frac{\hbar \Omega_{S,p}}{k_B T}} - 1} + 1, \tag{3}$$

where $\hbar$ is the reduced Planck constant, $\Omega_{AS,p}$ and $\Omega_{S,p}$ are the spectral detunings between the pump and the AS and S frequencies, respectively, and k_B is the Boltzmann constant [11]. By

Optics EXPRESS

assuming that the spectral detuning is frequency independent ($\Omega_{AS,p} = \Omega_{S,p} = \Omega$), the ratio of the AS to the S signal, after subtraction of their corresponding dark count rates, is given by

$$\frac{I_{AS}(x) - DC_{AS}}{I_S(x) - DC_S} = C_1 e^{-\frac{\hbar\Omega}{k_B T}} + C_2, \tag{4}$$

where C_1 and C_2 are two calibration constants. In the Eq. (4) we have made the approximation $e^{(\alpha_S - \alpha_{AS})x} \approx 1$, justified by the small difference between the attenuation losses at the AS and S wavelengths ($\alpha_{AS} = 0.225$ dB km^{-1} and $\alpha_S = 0.210$ dB km^{-1}) [16] and a 500 m maximum fiber length. The constant C_1 includes all transmission losses as well as detection efficiencies along the AS and S channels. Precisely, if one considers the same Raman gain coefficient and filtering bandwidth at the AS and S wavelengths, C_1 corresponds to the ratio of η_{AS} to η_S. In contrast, C_2 is added to Eq. (4) to take into account the Rayleigh noise, as well as the deviation from the value of spectral Raman detuning $\Omega = 13$ THz reported in literature for silica fibers [17,18,19]. By using Eq. (4), one can calculate the temperature at a position x of the FUT as

$$T(x) = -\frac{\hbar\Omega}{k_B \ln\left(\frac{\frac{I_{AS}(x) - DC_{AS}}{I_S(x) - DC_S} - C_2}{C_1}\right)}, \tag{5}$$

Calibration measurements at known temperatures are needed to determine the values of the constants C_1 and C_2. Therefore, our RDTS works as a secondary thermometer, as it relies on the measurement of fixed temperatures obtained from another primary thermometer.

4. Results

4.1. Calibration

In Fig. 2(a) we show the OTDR traces obtained after 1 minute integration of S and AS signals backscattered from a SM FUT of 5 m length. For these measurements, laser pulses have around 95 mW peak power. Losses of 0.2 dB at the input of the fiber are due to the input FUT connector. A portion of around 1 m of the fiber has been warmed up to 89 °C. Corresponding to the heated portion of the fiber, the value of S and AS signals increases with respect to that at room temperature, indicated by a dashed line. The AS signal turns out to be much more sensitive to temperature than the S one.

To investigate the effect of temperature on the AS signal, we vary the temperature from 14 to 95 °C with steps of 5 - 10 °C (Fig. 2(b)). The signals at the different temperatures can be easily discriminated. Interestingly, the signal also decreases for temperatures that are lower than room temperature (23 °C), as for 14 °C. These measurements are used to calibrate our RDTS. By linear fitting the values of the ratios $\frac{I_{AS}(x) - DC_{AS}}{I_S(x) - DC_S}$ as a function of $e^{-\frac{\hbar\Omega}{k_B T}}$, we obtain the values of the constants $C_1 = (1.10 \pm 0.01)$ and $C_2 = (0.027 \pm 0.001)$. Notice that only two temperatures are sufficient to determine the value of the two calibrating parameters. The fact that the value of C_1 is larger than 1 shows that losses are slightly more important in the AS channel. The value of C_2 is around 3% that of C_1. Figure 2(c) shows the agreement between the temperatures measured by the RDTS and those obtained with the reference thermometer, as the experimental points align well on the red line indicating the perfect matching. By using standard uncertainty analysis, we obtain an uncertainty in the temperature measurement between 2 °C and 3 °C with 1 minute integration. The standard deviation of the values of S and AS signals at the same temperature are used as their uncertainties. Notice that Dyer *et al* [11] have reported a similar temperature uncertainty, but with a system based on EDFA amplifiers, that in our case can been avoided thanks to the SNSPDs high detection efficiency.

Optics EXPRESS

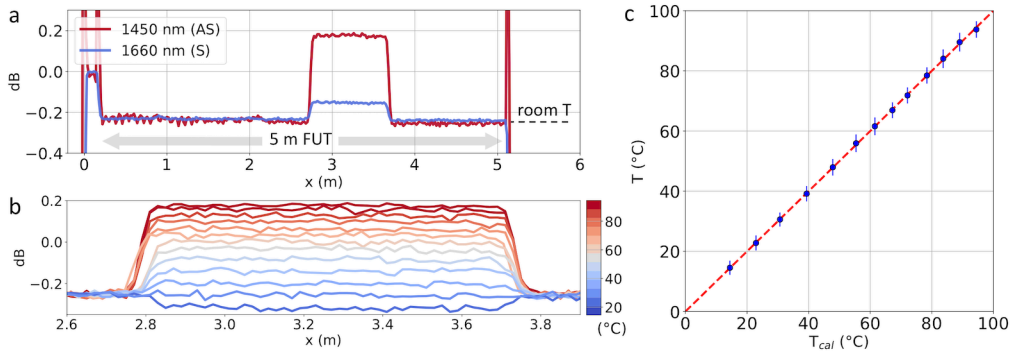

Fig. 2. Calibration of the RDTS on a 5 m FUT. a) Photon-counting OTDR traces associated to the Anti-Stokes (AS) and Stokes (S) Raman scattering signal. Corresponding to a portion of the FUT (around 1 m) which is heated up to 89°C, the value of the AS and S signals increase with respect to that at room temperature (dashed line). b) AS Raman signal corresponding to the heated portion of the FUT for different heating temperatures. c) Temperature values T measured by the RDTS (obtained after determining the calibration constants) as a function of those measured with the reference thermometer (T_{cal}). The red line indicates the perfect matching.

4.2. *Spatial resolution*

The spatial resolution of a DTS is related to the minimum distance over which a step change in temperature can be measured. We used two methods to determine the spatial resolution of the RDTS. The first consists in measuring the width of the temperature profile associated to a hot zone, i.e., a short heated portion of the FUT. In this case, the measured profile is directly associated to the convolution of the laser's pulse width with the response function of the detection system. The second is the 10-90 method, according to which the spatial resolution of a DTS is defined as the distance between 10% and 90% of its response to a sharp temperature step change [20].

As concerns the first approach, we have developed an electronic heating system to warm up hot zones of 1 cm length in the fiber. The OTDR trace corresponding to this zone incorporates all contributions that can degrade the spatial resolution, namely the detectors' jitter τ_{SNSPD}, the TDC timing uncertainty τ_{TDC}, as well as the pulse duration τ_{pulse}. We assume $\tau_{SNSPD} = 50$ ps [13] and $\tau_{TDC} = 28$ ps [21]. The temporal shape of our pulses depends on the power settings of the diode laser. In the intensity regime used for the measurements described in the previous section, the pulses have the temporal profile shown in Fig. 3(b), showing a $\tau_{pulse} = 250$ ps at FWHM. With these values we calculate the expected temporal ($\tau_{hot\ zone}$) and spatial spread ($\Delta l_{hot\ zone}$) associated to the hot zone as

$$\tau_{hot\ zone} = \sqrt{\tau_{SNSPD}{}^2 + \tau_{TDC}{}^2 + \tau_{1cm}{}^2 + \tau_{pulse}{}^2} \approx 280\ ps\ , \tag{6}$$

providing

$$\Delta l_{hot\ zone} = \frac{c\tau_{hot\ zone}}{2n} \approx 2.8\ cm, \tag{7}$$

where τ_{1cm} is the temporal spread due to the 1 cm hot zone and n is the optical fiber refractive index at the central wavelength of the laser source. Experimentally, we measure $\Delta l_{hot\ zone} = (3.3 \pm 0.3)$ cm at FWHM (Fig. 3(a), left box), in quite good agreement with the theoretical expectation. The main contribution to the measured value is provided by the pulse duration, the response function of the detection system being negligeable. In Fig. 3 we show the same measurement for lower

Optics EXPRESS

power settings of the laser diode, providing a pulse duration decreasing to around 50 ps (Fig. 3(b)). The spatial broadening of the hot zone turns out to be sensitive to the pulse width, achieving a value of (2.4 ± 0.3) cm at 50 ps FWHM pulse width (Fig. 3(a), right box), and confirming that the pulse width affects the most the spatial resolution. In this case, the measured $\Delta l_{hot\ zone}$ is around the double of what we expect with $\tau_{pulse} = 50$ ps. This discrepancy is probably due to the effective heated region in the fiber which could be larger than 1 cm because of heat diffusion. These results show that the detection system based on SNSPDs does not represent a limiting factor for the spatial resolution, which, in principle, could achieve the sub-centimeter scale.

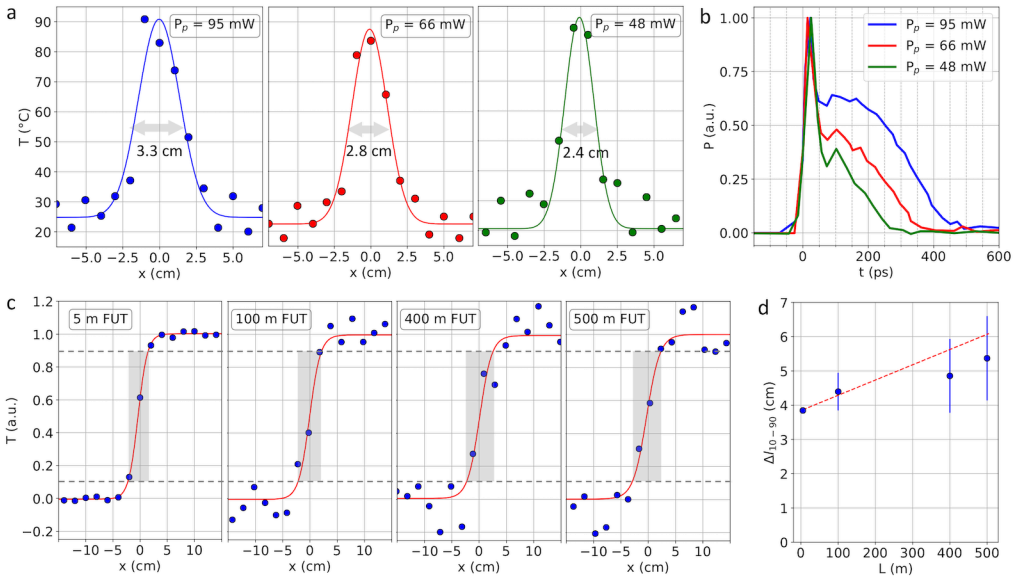

Fig. 3. Centimetric spatial resolution of the RDTS. a) RDTS temperature (T) profile associated to a 1 cm hot zone in a 5 m FUT for three laser pulse widths corresponding to the indicated peak power values P_p. Data points are fitted with gaussian functions (continuous curves). b) Temporal profile of the laser pulses at the different peak power values. c) Rising edge of the RDTS temperature profile with the 5 m, 100 m, 400 m, and 500 m FUT associated to around 1 m heated portion at the far fibers end. Data points are fitted with a logistic function (continuous red curves). Dashed lines indicate 10% and 90% of the RDTS response. Gray regions are those selected for the determination of the spatial resolution. d) Spatial resolution Δl_{10-90} determined with the 10-90 method as a function of FUT length L. The red dotted line corresponds to the expected change of spatial resolution due to AS and S chromatic dispersion during back propagation (Eq. (8)).

We also measure the spatial resolution of our RDTS via the 10-90 method. A temperature step change has been measured in the high peak power regime for the 5 m FUT (Fig. 3(c), first box). The temperature profile has been fitted with a logistic function. We measured a spatial resolution of $\Delta l_{10-90} = (3.8 \pm 0.1)$ cm, in good agreement with the measured value of $\Delta l_{hot\ zone}$, as the resolution measurable with the 10-90 method provides in principle a value around 20% larger. Notice that we do not fully exploit the potential of SNSPDs, as their timing jitter could allow even sub-centimeter resolution. A spatial resolution of 2-3 cm could be in principle achieved even by free running single photon avalanche detectors (SPADs) with 150–200 ps timing jitter. However, for a similar dark counts rate (~100 Hz), SPADs typically have much lower efficiency (~20% with respect to ~70%) and much longer dead-time (~10 µs with respect to < 100 ns), providing a dramatic decrease of the Signal-to-Noise ratio (SNR) and, therefore, of the temperature resolution.

Optics EXPRESS

We adopt the 10-90 method to understand how spatial resolution of the RDTS changes with the length of the FUT and we test fibers of 100 m, 400 m, and 500 m length that have been warmed up at their far end. Photon counts are integrated over one minute for the 5 m FUT, and 3 minutes for the other FUT lengths. We observe an increase of Δl_{10-90}, so a reduction of the spatial resolution, for an increasing FUT length (Fig. 3(d)). As the SNR of the RDTS traces gets worse with long fibers, the uncertainty on Δl_{10-90} increases with distance. We attribute the increment in Δl_{10-90} to the chromatic dispersion experienced by S and AS pulses during their back propagation in the FUT, which is non negligible as their bandwidth $\Delta\lambda_{AS,S}$ is around 20 nm. In contrast, dispersion of laser pulses at 1548 nm is negligible as the laser linewidth is around 1.5 nm. Therefore, we expect that the increase in Δl at a fiber length L can be written as

$$\Delta l_L - \Delta l_{5m} = CD_{AS,S}\Delta\lambda_{AS,S}\frac{c}{n}L\,, \tag{8}$$

where Δl_{5m} is the spatial resolution for the 5 m FUT, and $CD_{AS,S}$ the average chromatic dispersion at 1450 nm and 1660 nm (~15 ps nm^{-1} km^{-1}). In Fig. 3(d) a red dotted line corresponding to Eq. (8) represents the expected increase in Δl_{10-90}, which is in good agreement with the experimental points and their uncertainties. The change in spatial resolution turns out to be around 4 cm per km length.

4.3. Temperature resolution

The temperature resolution of a DTS is the degree of uncertainty in the temperature information and strongly depends on the SNR of the OTDR traces, which is affected by many factors, such as the efficiency of the detectors, the integration time, and the binning size of the photon counts. We first analyze the SNR of the OTDR traces in combination with spatial averaging of the measured data, obtained by increasing the binning size. In Fig. 4(a) we show how the SNR value, calculated as the ratio of the average signal over its standard deviation [10], changes with spatial data averaging. Error bars get generally larger for long bin sizes as less data are used to calculate the SNR. We perform the same analysis for 5 m, 100 m, 400 m, and 500 m FUT. Photon counts are integrated over one minute for the 5 m FUT, and 3 minutes for the other fiber lengths.

In all cases, the SNR increases with a square root dependence on photon counts and achieves an asymptotic value at around 20 cm bin size. As expected, the SNR mean value decreases as a function of the FUT length (Fig. 4(b)), mainly because the repetition rate of the laser needs to be reduced for long fibers. We calculated the expected drop in SNR with respect to the value obtained for the 5 m FUT. To this end, we use the expression found in [10] for photon counting OTDR, according to which

$$SNR = \frac{P\sqrt{t}\sqrt{f}}{NEP\ \sqrt{B}}\,, \tag{9}$$

where P is the scattered optical power, f the repetition rate of the laser, NEP the SNSPD noise-equivalent-power, and B the detection bandwidth. We name SNR_{5m} the SNR measured with a 5 m FUT at a repetition rate f_{5m}. By changing the repetition rate from f_{5m} to f_L, which is the repetition rate at fiber length L, the optical power changes by a factor $\frac{f_L}{f_{5m}}P_{5m}$. By assuming that the NEP and B are not altered by the change in repetition rate, the ratio between the SNR at fiber length L, SNR_L, and SNR_{5m} can be written as

$$\frac{SNR_L}{SNR_{5m}} = \sqrt{\frac{t_L}{t_{5m}}}\left(\frac{f_L}{f_{5m}}\right)^{\frac{3}{2}}, \tag{10}$$

where $t_{5m(L)}$ is the integration time at 5 m (L) fiber length. As shown in Fig. 4(b), the calculated values of SNR are in quite good agreement with the experimental results.

Optics EXPRESS

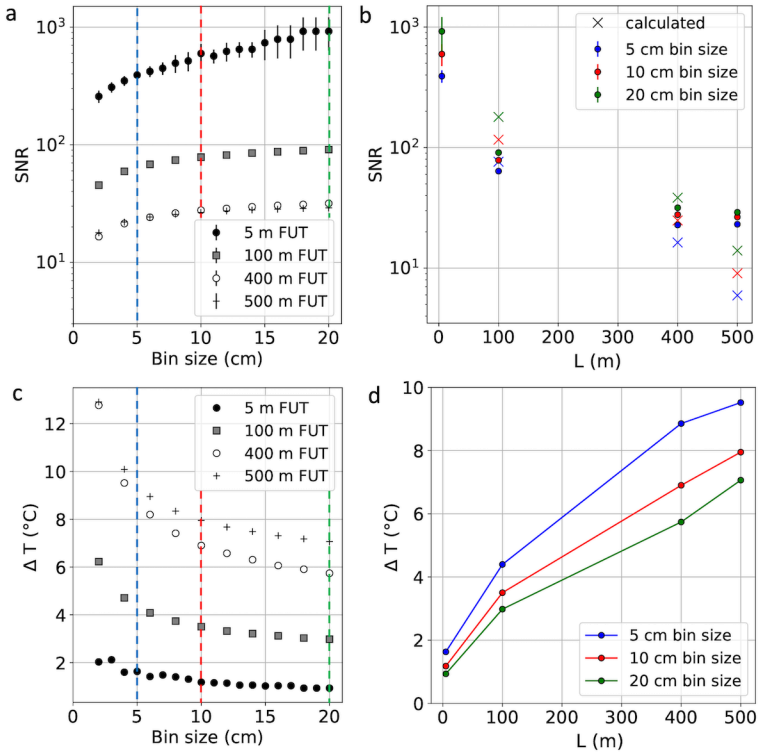

Fig. 4. Temperature resolution of the RDTS as a function of spatial averaging and FUT length. a, b) Mean Signal-to-Noise ratio (SNR) in logarithmic scale as a function of bin size for different FUT lengths (a) and fiber length L for 5, 10 and 20 cm bin size. Dashed lines indicate the values at the selected bin sizes. c, d) RDTS temperature resolution ΔT as a function of bin size (c) and of fiber length L (d). Lines connecting the experimental points are used to guide the eyes.

We now estimate the temperature resolution of the RDTS by calculating the standard deviation ΔT of a single temperature trace at a certain temperature. In this case we still perform spatial averaging to understand what can be gained in temperature resolution at the detriment of spatial resolution. By increasing the binning size, ΔT decreases, so the temperature resolution increases, and achieves an asymptotic value due to the statistical saturating effect in the SNR. For the 5 m FUT, we measure 1.5 °C temperature resolution with 5 cm bin size and 1 minute integration (Fig. 4(c)). The high efficiency of the adopted SNSPDs allows to reduce the overall optical losses with increase of the SNR and to achieve a temperature resolution similar to what is obtained in [11]. Temperature resolution degrades with fiber length because of reduction of the SNR, due to the decrease of the laser repetition rate. In Fig. 4(d), we show the temperature resolution for 5, 10 and 20 cm bin size for different fiber lengths. At 500 m fiber length, temperature resolution is around 8 °C with 10 cm bin size and 3 minutes integration.

5. Conclusions

In this work, we demonstrate a RDTS based on telecom SM fibers and efficient SNSPDs showing around 3 cm spatial and 1.5 °C temperature resolution on a 5 m FUT with only 1 min integration. We have shown that spatial resolution is limited by the pulse width and not by the detection system, so that in principle sub-centimeter spatial resolution could be achieved. The high

Optics EXPRESS

detection efficiency of the adopted SNSPDs allows to strongly simplify the optical setup of the RDTS, by avoiding the need of EDFA amplification to achieve a high SNR. Thanks to the spiral geometry of the superconducting nanowire, the adopted SNPSDs are polarization independent. This property allows to avoid additional optical components in the RDTS, such as polarization diversity receivers, as well as systematic uncertainties due to polarization. We have tested our RDTS on fibers up to 500 m length. For long fibers, we have observed that the spatial resolution decreases in such a way that the minimum distance for a measurable temperature step change increases of around 4 cm per km length, because of chromatic dispersion of Stokes and Anti-Stokes photons during their back-propagation in the FUT.

As the repetition rate of the pump laser needs to be lowered for long fibers, the SNR gets worse at long distances and temperature resolution decreases for short integration times. However, we measure 10 cm spatial and 8 °C resolution on a 500 m fiber with 3 minutes integration and confirm the possibility to perform temperature measurements with a spatial resolution at the cm scale. Some techniques are known to enhance SNR in OTDR at the cost of a certain complexification of the device. For instance, pseudo-random pulse sequences can be sent into the FUT, and correlate the backscattered signal to these sequences [22].

In this work, we demonstrate the feasibility of RDTS with centimetric resolution on hundreds of meters sensing range. These results could pave the way for a new kind of applications that do not currently adopt distributed temperature sensing. For instance, these performances could be exploited to map temperature over surfaces and volumes, especially in systems where a dense network of point sensors is spatially hard to install or where the absence of electromagnetic interference is highly desirable, such as complex electronic circuits, particle detectors for high energy physics, cryogenic devices, automotive engines, and aerospace vehicles components such as airplane wings.

Funding. Haute école Spécialisée de Suisse Occidentale.

Acknowledgements. We would like to thank Marc Nikles and Cédric Schmidt for useful discussions. We are also thankful to Olivier Masson for technical support.

Disclosures. The authors declare no conflicts of interest.

Data availability. Data underlying the results presented in this paper are not publicly available at this time but may be obtained from the authors upon reasonable request.

References

1. M. K. Barnoski and S. M. Jensen, "Fiber waveguides: a novel technique for investigating attenuation characteristics," Appl. Opt. **15**(9), 2112 (1976).
2. J. P. Dakin, D. J. Pratt, G. W. Bibby, and G. N. Ross, "Distributed optical fiber Raman temperature sensor using a semiconductor light source and detector," Electron. Lett. **21**(13), 569 (1985).
3. L. Thévenaz, "Review and progress in distributed fiber sensing," Optical Fiber Sensors, OSA Technical Digest (CD) (Optical Publoshing Group, 2006), paper ThC1.
4. M. Wang, H. Wu, M. Tang, Z. Zhao, Y. Dang, C. Zhao, R. Liao, W. Chen, S. Fu, C. Yang, W. Tong, P. P. Shum, and D. Liu, "Few-mode fiber based Raman distributed temperature sensing," Opt. Express **25**(5), 4907 (2017).
5. Y. Liu, L. Ma, C. Yang, W. Tong, and Z. He, "Long-range Raman distributed temperature sensor with high spatial and temperature resolution using optimized graded-index few-mode fiber over 25 km-long distance," Opt. Express **26**(16), 20562 (2018).
6. J. Li, Q. Zhang, Y. Xu, M. Zhang, J. Zhang, L. Qiao, M. M. Promi, and T. Wang, "High-accuracy distributed temperature measurement using difference sensitive-temperature compensation for Raman-based optical fiber sensing," Opt. Express **27**(25), 36183 (2019).
7. G. Bolognini, J. Park, M. A. Soto, N. Park, and F. Di Pasquale, "Analysis of distributed temperature sensing based on Raman scattering using OTDR coding and discrete Raman amplification," Meas. Sci. Technol. **18**(10), 3211–3218 (2007).
8. G. N. Gol'tsman, O. Okunev, G. Chulkova, A. Lipatov, A. Semenov, K. Smirnov, B. Voronov, and A. Dzardanov, "Picosecond superconducting single-photon optical detector," Appl. Phys. Lett. **79**(6), 705–707 (2001).
9. I. Esmaeil Zadeh, J. Chang, J. W. N. Los, S. Gyger, A. W. Elshaari, S. Steinhauer, S. N. Dorenbos, and V. Zwiller, "Superconducting nanowire single-photon detectors: A perspective on evolution, state-of-the-art, future developments, and applications," Appl. Phys. Lett. **118**(19), 190502 (2021).

Optics EXPRESS

10. P. Eraerds, J. Zhang, H. Zbinden, N. Gisin, and M. Legré, "Photon Counting OTDR: Advantages and Limitations," J. Lightwave Technol. **28**(6), 952–964 (2010).
11. S. D. Dyer, M. G. Tanner, B. Baek, R. H. Hadfield, and S. W. Nam, "Analysis of a distributed fiber-optic temperature sensor using single-photon detectors," Opt. Express **20**(4), 3456 (2012).
12. T. D. Vo, J. He, E. Magi, M. J. Collins, A. S. Clark, B. G. Ferguson, C. Xiong, and B. J. Eggleton, "Chalcogenide fiber-based distributed temperature sensor with sub-centimeter spatial resolution and enhanced accuracy," Opt. Express **22**(2), 1560 (2014).
13. M. Caloz, M. Perrenoud, C. Autebert, B. Korzh, M. Weiss, C. Schönenberger, R. J. Warburton, H. Zbinden, and F. Bussières, "High-detection efficiency and low-timing jitter with amorphous superconducting nanowire single-photon detectors," Appl. Phys. Lett. **112**(6), 061103 (2018).
14. X. Li, P. L. Voss, J. Chen, K. F. Lee, and P. Kumar, "Measurement of co- and cross-polarized raman spectra in silica fiber for small detunings," Opt. Express **13**(6), 2236 (2005).
15. L. de la Cruz-May, E. B. Mejìa, O. Benavides, J. Vásquez Jiménez, J. Castro-Chacón, and M. May-Alarcón, "Novel Technique for Obtaining the Raman Gain Efficiency of Silica Fibers," IEEE Photonics J. **5**(4), 6100305 (2013).
16. M. S. P. Silva, H. P. Alves, J. F. Do Nascimento, and J. F. Martins-Filho, "Impact of pulse width on the sensitivity and range of a raman-based distributed fiber-optic temperature sensor," J. Microwaves, Optoelectron. Electromagn. Appl. **17**(4), 539–551 (2018).
17. D. Mahgerefteh, D. L. Butler, J. Goldhar, B. Rosenberg, and G. L. Burdge, "Technique for measurement of the Raman gain in optical fibers," Opt. Lett. **21**(24), 2026 (1996).
18. M. Koeppel, S. Werzinger, T. Ringel, P. Bechtold, T. Thiel, R. Engelbrecht, T. Bosselmann, and B. Schmauss, "Combined distributed Raman and Bragg fiber temperature sensing using incoherent optical frequency domain reflectometry," J. Sens. Sens. Syst. **7**(1), 91–100 (2018).
19. L. Schenato, "A review of distributed fiber optic sensors for geo-hydrological applications," Appl. Sci. **7**(9), 896 (2017).
20. N. Simon, O. Bour, N. Lavenant, G. Porel, B. Nauleau, B. Pouladi, and L. Longuevergne, "A comparison of different methods to estimate the effective spatial resolution of FO-DTS measurements achieved during sandbox experiments," Sensors **20**(2), 570 (2020).
21. *ID900 Time Controller datasheet*, www.idquantique.com
22. G. D. Brinatti Vazquez, O. E. Martínez, and D. Kunik, "Distributed Temperature Sensing using Cyclic Pseudorandom Sequences," IEEE Sensors J. **17**(6), 1686–1691 (2017).